Transmission Electron Microscopy

S J Pennycook, Oak Ridge National Laboratory, Oak Ridge, TN, USA

Published by Elsevier Ltd.

Introduction

The distinguishing feature of transmission electron microscopy (TEM) is its ability to form images of atomic arrangements at localized regions within materials. It provides a view of the microstructure, that is, the variations in structure from one region to another, and the interfaces between them. TEM plays a critical role whenever macroscopic properties are controlled or influenced by defects or interfaces, for example, in the development of advanced structural materials with their complex microstructure of second phases or electronic materials which rely on the exquisite control of interfaces and multilayers. X-ray or neutron diffraction provide quite complementary information. These techniques can determine the average structure of complex materials very precisely, but not the structure of a local region or individual nanostructure. As condensed matter physics moves toward the study of ever more complex materials, and at the same time interest in nanoscale physics and devices is increasing, TEM or its scanning counterpart STEM, is finding a rapidly increasing role in basic condensed matter physics research.

The unique role of the TEM arises because electrons are charged particles, and therefore, unlike X-rays or neutrons, are able to be accelerated and precisely focused by electromagnetic fields. The scattered beams can be collected by a lens, and refocused to form a true real space image in the manner of an optical microscope, where each point in the image corresponds to a specific point in the object. Electrons also interact much more strongly with matter and electron diffraction can be performed on materials of nanometer dimensions. For accelerating voltages of 100–1000 kV, the electron wavelength ranges from 0.004 to 0.001 nm, orders of magnitude lower than atomic spacings in materials. It would therefore appear relatively trivial to form atomic resolution images of materials. However, it is only very recently that atomic resolution imaging could be said to be at all trivial. The major limitation was realized early in the history of the microscope to be the high inherent aberrations of a round magnetic lens. Spherical aberration is the dominant aberration, and leads to a ray deviation of $C_s\alpha^3$, where α is the semiangle of the objective lens. With electron lenses, C_s is of the same order as the focal length. This means that only very small apertures could be used, and since microscope resolution is given by $0.61\lambda/\sin\alpha$, where λ is wavelength, the best resolution would be limited by diffraction to $\sim 50\lambda$.

It took ~ 50 years from the development of the first transmission electron microscopes in the 1930s to achieve sufficient electrical and mechanical stability to allow imaging of crystal lattices at 0.2–0.3 nm resolution in the 1980s. Over the next 20 years, resolution improved incrementally to 0.1–0.2 nm. Now electron microscopy is in the midst of a revolution. Thanks to the development of solid-state devices, specifically the computer and charge-coupled-device (CCD) detectors, a series of nonround magnetic lenses can be used to correct the aberrations of the (round) objective lens. The gain in resolution over the last few years is comparable to that seen in the last few decades, an extraordinary advance that has pushed TEM into the sub-Ångstrom regime for the first time in history.

Aberration-correction brings more than just resolution; better resolution brings increased sensitivity, and recent results have demonstrated the imaging of single atoms within materials and on their surfaces, together with their spectroscopic identification by electron energy loss spectroscopy (EELS). Furthermore, entirely new modes of microscopy now appear feasible. Aberration-correction is allowing the objective aperture to be opened up, and, just as in an optical microscope, the depth of focus reduces. We are seeing the beginnings of three-dimensional (3D) TEM.

Electron Optics of the Microscope: STEM Versus TEM, Reciprocity

Figure 1a shows a schematic ray diagram for conventional TEM. The specimen is illuminated through a condenser aperture and transmitted electrons are gathered by the objective lens and recombined into an image. Historically, the size of the condenser aperture has always been chosen to be as small as practically possible to provide a close approximation to parallel illumination. This is required for diffraction contrast imaging, when only one diffracted beam is passed through the objective aperture. With parallel illumination crystal defects such as dislocations, precipitates, and interfaces are observable, and many details of their atomic structure can be obtained by detailed analysis of image contrast (e.g., lattice shifts across an interface, the

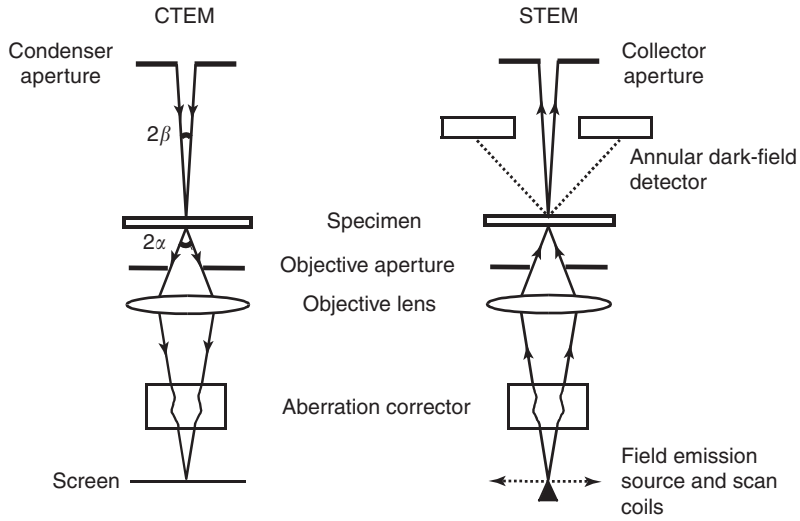

Figure 1 Ray diagrams for (a) the TEM and (b) the STEM, showing the reciprocal nature of the optical pathways. The TEM image is obtained in parallel, the STEM image pixel by pixel by scanning the probe. The STEM also provides simultaneous annular dark-field (ADF) imaging. Actual microscopes have several additional lenses and the beam limiting aperture positions may differ.

intrinsic or extrinsic nature of stacking faults, coherency strains of precipitates, Burgers' vectors of dislocations). Nearly parallel illumination provides a long coherence length in the specimen, approximately λ/β, where β is the illumination semiangle. For small β many lattice spacings are illuminated in phase, an example of coherent imaging. If the objective aperture α is opened up to include several diffracted beams, the conventional TEM lattice-imaging mode is obtained, often known as high-resolution electron microscopy (HREM), another example of coherent imaging.

In scanning transmission electron microscopy (STEM) the electron beam is focused to a small probe and scanned across the specimen. **Figure 1b** shows the ray diagram; detectors are used to pick up a signal, which is used to form an image pixel by pixel as the probe is scanned. The STEM allows complete flexibility in choice of detector, and multiple detectors are normally used giving complementary information. An annular dark field (ADF) detector collects electrons scattered out of the beam and gives an image of mass thickness, that is, a signal that increases with increasing scattering cross section and specimen thickness; a hole appears dark. A bright-field signal can also be detected using an on-axis detector (holes appear bright). If the bright-field detector subtends a small angle β at the specimen, then it is clear from comparing the two ray diagrams in **Figure 1** that the only difference in the optics of the two forms of microscope is the direction of the electron beam. The major source of image contrast is elastic scattering, for which only the scattering angle is important not the direction of propagation (an example of time-reversal symmetry). This illustrates the principle of reciprocity, where interchange of source and detector leads to the same image, and explains why images formed in bright-field STEM may show identical contrast behavior to those in TEM. If the bright-field collector aperture is small, these images are coherent images exactly equivalent to bright-field TEM images.

Reciprocity applies even if aberration correctors are added to both columns. In TEM the corrector is placed after the specimen to correct the objective lens aberrations, while in STEM it is placed before the specimen, the purpose being again to correct the aberrations of the objective lens (now used as a probe-forming lens). **Figure 1** makes clear that for the same set of aberration parameters and equivalent angles before and after the specimen, the same images are to be expected, and this is seen experimentally. However, reciprocity does not mean the images will have the same signal-to-noise ratio. Before aberration-correction, the angle β necessary to ensure good coherent imaging conditions was so small that the STEM image used only a small fraction of the electrons passing through the specimen. This resulted in noisy images and unnecessary specimen irradiation. With aberration-correction, not only can the objective aperture α be made much larger, but β can also be increased and STEM bright-field imaging becomes a useful practical possibility.

The primary motivation for the STEM has been its ability to detect signals other than the bright-field image, in particular, the ADF image. Based on the concept of a coherence width in the specimen, if the angle β is sufficiently large, the coherence width in

the specimen is below the typical atomic spacings in materials. Although the third dimension along the beam direction must also be considered, the ADF image does represent a good approximation to incoherent imaging. An incoherent image gives a simple relationship between the object and image as in a camera, and is easier to interpret than a coherent image. The very different characteristics of coherent and incoherent imaging will be discussed in the next section.

Finally, one of the major uses of STEM has been for microanalysis, which uses one or more additional signals generated as the beam passes through the specimen. Perhaps the most important of these is inelastic scattering, which allows elemental identification from inner-shell excitations. The fine structure at the absorption edges carries information about the electronic structure of the excited atom. For these purposes, EELS is comparable to X-ray absorption spectroscopy, but is available with the spatial resolution of the probe. Spectroscopy of individual atomic columns in a crystal has been demonstrated, including, recently, the spectroscopic identification of a single impurity atom within one atomic column. In the so-called spectrum-imaging mode, one complete spectrum is recorded for each pixel in the image. Similar information can be obtained on a TEM using an imaging filter, which produces 2D images corresponding to particular energy losses. A set of such images at different energy losses is somewhat equivalent to a spectrum image on the STEM. However, reciprocity does not apply to inelastic scattering and there are important differences between TEM and STEM: in the TEM the inelastically scattered electrons must be focused by the image-forming lens which leads to problems with chromatic aberration, whereas in the STEM there are no lenses after the specimen. For this reason atomic column resolution has yet to be achieved in the TEM.

Energy dispersive X-ray spectroscopy, known as EDX or EDS, collects X-rays emitted as the atom relaxes into its ground state following inner-shell excitation, and the X-ray energy is again characteristic of the element. The peak resolution is much lower than for EELS, but the peaks lie on a lower background. The major problem is the low efficiency of collection. X-rays are emitted over 4π steradians and only a small fraction can be collected by the detector, whereas the corresponding core loss electrons are forward peaked and a high fraction can be collected for EELS. This is probably the reason that atomic-resolution EDX analysis has yet to be demonstrated. Other possible imaging signals include the secondary electrons for imaging surfaces and visible photons (cathodoluminescence) for mapping optical properties.

Finally, microdiffraction, or more recently nanodiffraction patterns can be recorded with an imaging detector in STEM. This is very useful for identifying minority phases within bulk materials or new phases not possible to synthesize in large volumes, and also for quantitative measurements of charge modulation. For long wavelength modulations, electron diffraction is much more sensitive than X-ray diffraction because of the cancellation of the scattering due to the electrons and nucleus; electron scattering sees the imbalance of charge, whereas X-ray scattering sees the total electron density and is less sensitive to small changes.

For much of the history of electron microscopy it has not been possible to have high-resolution STEM and TEM imaging in a single machine. In recent years however, great advances have been made in instrument design, and it is now possible to purchase microscopes that will give good performance in any desired mode of operation, often simply at the push of a button. It is possible today to purchase an instrument with two aberration-correctors, one before the specimen to correct the probe and one after the specimen to provide parallel-detection phase contrast imaging.

Principles of Image Formation

Coherent Imaging

With parallel illumination, a crystal aligned near a zone axis will generate a set of diffracted beams leaving the sample at specific angles, as depicted in **Figure 2a**. The objective lens brings these beams to a focus in its back focal plane to form the diffraction pattern. In diffraction contrast imaging, one diffracted beam is passed through a small objective aperture and the resulting image represents a map showing the distribution of diffracted intensity from the specimen. The crystal lattice is unresolved, but the image is useful for studying defects and interfaces. To resolve the crystal lattice itself the objective aperture is opened up to include more than one diffracted beam. Now each point in the image receives contributions from multiple diffracted beams that interfere to generate image contrast, which depends on their relative phases. The principles of coherent phase contrast lattice imaging are best illustrated for the idealized case of a thin sample where multiple scattering can be ignored. The incident electron wave function takes the form of a plane wave ψ_0 which interacts with the electrostatic potential of the specimen $\phi(r)$ (ignoring magnetic fields for now). Here, lowercase letters refer to 3D variables while upper case variables refer to the two transverse dimensions

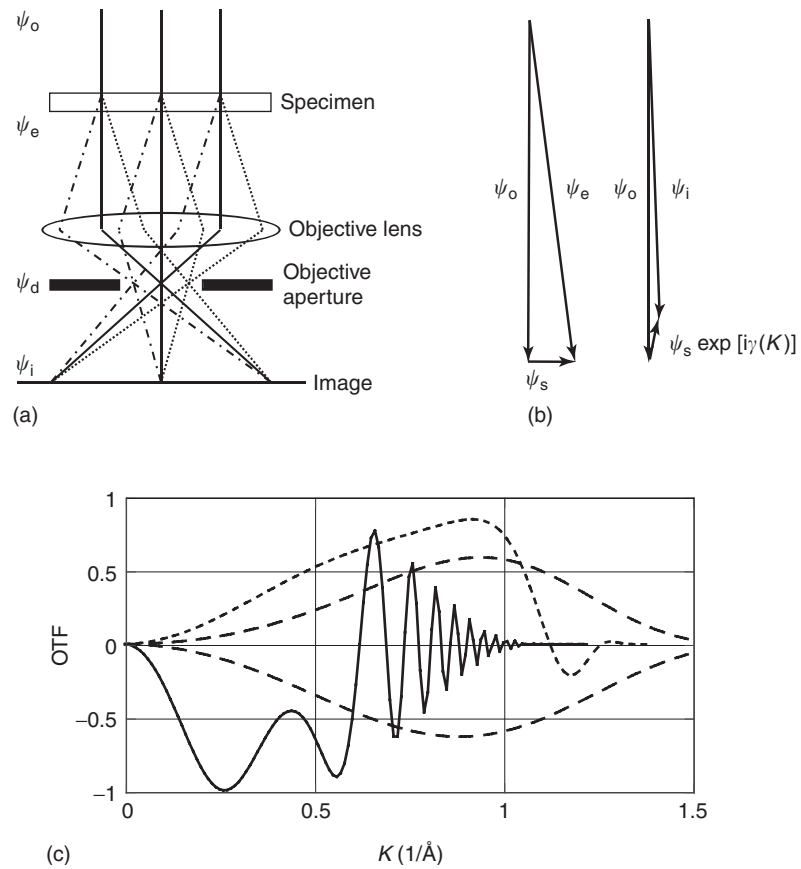

Figure 2 (a) Ray diagram for coherent phase contrast imaging of a crystal. Diffracted beams emerge from the specimen at specific angles and are brought to a focus in the back focal plane of the objective lens. They are recombined in the image plane. Imaging is therefore two consecutive Fourier transforms. (b) Vector diagram for a weak phase object showing the incident beam, a small scattered beam with $\pi/2$ phase change and the resultant transmitted beam. Lens aberrations are used to rotate the phase of the scattered beam an additional $\pi/2$ to create amplitude contrast from the phase changes. (c) Contrast transfer functions for an uncorrected 300 kV microscope, solid line ($C_s = 0.6$ mm, $\Delta f = -45$ nm, energy spread 2 nm typical for a Schottky field emission source), a corrected 300 kV microscope, dotted line ($C_s = -37\,\mu$m. $C_5 = 100$ mm, $\Delta f = 5$ nm, energy spread 1 nm typical for a cold field emission source), and a 200 kV microscope with full correction of all 5th-order aberrations, dashed line ($C_s = 23\,\mu$m. $C_5 = -2$ mm, $C_7 = 100$ mm, energy spread 1 nm). The upper trace is for $\Delta f = 1$ nm giving white atom contrast in a thin specimen, the lower one is for $\Delta f = -2$ nm giving black atoms.

normal to the direction of beam propagation, z; for example the position vector $\boldsymbol{r} = (R, z)$ and the electron wave vector $\boldsymbol{k} = (K, k)$. Assuming an incident beam of unit amplitude, a thin specimen acts as a weak phase grating, refracting the incident beam but not changing its amplitude: the exit face wave function is given by

$$\psi_e(\boldsymbol{R}) = \exp\{-i\sigma\phi(\boldsymbol{R})\} \approx 1 - i\sigma\phi(\boldsymbol{R})$$

where $\sigma = 2\pi me\lambda/h^2$ is the interaction constant and $\phi(\boldsymbol{R}) = \int \phi(r)\,dz$ is the projected potential. Phase changes in the exit wave therefore map the projected potential of the specimen. These phase changes can be represented vectorially by generation of a scattered wave $\psi_s(\boldsymbol{R}) = -i\sigma\phi(\boldsymbol{R})$ which is oriented at $\pi/2$ to the incident wave, as shown in **Figure 2b**. Entering the objective lens, the diffracted amplitude ψ_d is just the Fourier transform of the exit face wave function

$$\psi_d(\boldsymbol{K}) = \delta(0) - i\sigma\phi(\boldsymbol{K})$$

where the delta function at $\boldsymbol{K} = 0$ is just the unscattered beam. For a crystal aligned to a zone axis the diffraction pattern consists of a set of sharp diffracted beams at specific directions ($\boldsymbol{K}$ vectors). With a pure phase object, none of the individual diffracted beam intensities shows an image. To form an image of ψ_s, the diffracted beams must be passed through the objective lens and interfered with the unscattered beam. As shown in **Figure 2b**, the phase of the scattered beams should ideally be rotated an additional $\pi/2$ to convert the phase changes to perfect amplitude contrast. In this ideal case the image amplitude would become $\psi_i(\boldsymbol{R}) = 1 \pm \sigma\phi(\boldsymbol{R})$ and the intensity $I(\boldsymbol{R}) = |\psi_i(\boldsymbol{R})|^2 = 1 \pm 2\sigma\phi(\boldsymbol{R})$, depending on the

sense of rotation of the scattered wave with respect to the unscattered wave. In practice, since there are no phase plates for electrons, the only available source of additional phase changes are lens aberrations and defocus. The phase change introduced by the objective lens is referred to as the transfer function phase factor exp $[\mathrm{i}\gamma(\boldsymbol{K})]$ where

$$\gamma(K) = \pi\left(\Delta f \lambda K^2 + \tfrac{1}{2}\, C_3 \lambda^3 K^4 + \tfrac{1}{3}\, C_5 \lambda^5 K^6\right)$$

if only the rotationally symmetric aberrations are included so that $K = |\boldsymbol{K}|$. Here Δf is defocus, C_3 is the third-order spherical aberration coefficient, usually referred to simply as C_s before aberration-correction became viable, with typical values of the order of 1 mm. Now that C_s can be corrected, the fifth-order spherical aberration coefficient C_5 takes over as the limiting aberration. The diffraction amplitude transmitted by the lens becomes

$$\psi_{\mathrm{d}}(\boldsymbol{K}) = \delta(0) - \mathrm{i}\sigma\phi(\boldsymbol{K})\, \exp[\mathrm{i}\gamma(\boldsymbol{K})]$$

and for small phase changes the intensity becomes

$$I(\boldsymbol{R}) = 1 - 2\sigma\phi(\boldsymbol{R}) \otimes f(\sin\gamma(\boldsymbol{K}))$$

The phase changes $\phi(\boldsymbol{K})$ contribute to the image with a contrast given by $\sin\gamma(\boldsymbol{K})$, which is therefore referred to as the phase contrast transfer function, and the image is given by a convolution of the projected potential with the Fourier transform of $\sin\gamma(\boldsymbol{K})$.

The different aberrations depend on spatial frequencies to different powers and can therefore only be balanced over a finite range. **Figure 2c** shows examples for some uncorrected and aberration-corrected microscopes. Note that phase contrast imaging provides no contrast at zero spatial frequency because there is negligible additional phase change from lens aberrations. The uncorrected microscope shows rapid contrast oscillations at high spatial frequencies where the $C_s K^4$ term increases very rapidly; such oscillations are largely avoided in the corrected microscopes. The substantial drop in contrast at high spatial frequencies is due primarily to the finite energy spread of the beam. In this regard, the cold field emission gun is preferable to the Schottky thermal field emission gun. One characteristic of phase contrast is immediately apparent. The defocus phase factor is used to balance the dominant term in spherical aberration, but changes sign either side of Gaussian focus. In many cases, it is possible to reverse the image contrast on changing the focus (see **Figure 2c**) and atoms may look black or white in a phase contrast image. This can also happen if the specimen becomes thicker and additional relative phase changes occur between the diffracted beams due to dynamical diffraction (multiple scattering). The exit face wave function no longer relates simply to projected potential and becomes increasingly nonlocal. The general expression for the image intensity is

$$I(\boldsymbol{R}) = |\psi_{\mathrm{e}}(\boldsymbol{R}) \otimes P(\boldsymbol{R})|^2$$

the square of a convolution of the exit face wave function with the point response function of the objective lens. The point response function is just the Fourier transform of the transfer function phase factor,

$$P(\boldsymbol{R}) = \int A(\boldsymbol{K}) \mathrm{e}^{2\pi \mathrm{i} \boldsymbol{K}\cdot\boldsymbol{R}} \mathrm{e}^{\mathrm{i}\gamma(\boldsymbol{K})}\, \mathrm{d}\boldsymbol{K}$$

where $A(\boldsymbol{K}) = 1$ over the range of the objective aperture. Because the image is given by a square of the convolution, sum and difference spatial frequencies can appear, and for these reasons image simulations are normally required to relate a phase contrast image to an object.

Incoherent Imaging

Incoherent imaging provides a simple relationship between the object and image

$$I(\boldsymbol{R}) = O(\boldsymbol{R}) \otimes |P(\boldsymbol{R})|^2$$

where the object $O(\boldsymbol{R})$ is blurred by the resolution function of the imaging device. Strictly, this applies only when each point on the object emits independently of its neighbors so that there are no permanent phase relationships between them and no persistent interference can occur. The coherence length of the Sun on Earth is ~ 0.02 mm, so that observation on a larger length scale is effectively incoherent. This is the kind of imaging familiar from the camera, for example, where changing focus merely blurs the image but does not invert the contrast. It also applies to optical microscopy if a large aperture condenser lens is used to give effectively incoherent illumination, as first analyzed by Lord Rayleigh in 1895.

In the STEM, $|P(\boldsymbol{R})|^2$ is the intensity profile of the probe (see **Figure 1b**). Not every image takes the form of a simple convolution, as seen already for the case of the small axial detector. The requirement for an incoherent image is that all of the scattering (or other generated signal) be collected by the detector. In the case of inelastic scattering or X-ray emission, it is relatively simple to collect all of the signal, or at least a representative fraction of it. In the case of

elastically scattered electrons it is not so obvious, because collecting all of the transmitted electrons will give no image contrast; the specimen does not absorb any electrons, it only scatters them, and partial detection of the scattering is therefore necessary to generate an image.

The reason that collecting all of the scattering results in an incoherent image is that the detected signal is then insensitive to any interference that may be occurring amongst different scattered beams. Interference rearranges intensity but the total scattering is constant, by conservation of energy. The annular detector provides a close approximation to incoherent imaging because it can be arranged to average over a large number of diffracted beams. The inner detector angle should also be large to avoid being dominated by a few low-order beams around the inner hole. In practice, the image still shows strong incoherent characteristics even if the inner angle is just larger than the objective aperture angle, which is a mode that gives highly efficient dark-field imaging of single atoms and was the original motivation for the introduction of the detector by Crewe and co-workers.

High-angle scattering comes from the sharpest part of the atomic potential, the nucleus, and its intensity is proportional to the square of atomic number (Z). An annular detector with a large hole therefore gives an image showing strong Z-contrast, also referred to as a high-angle annular dark-field (HAADF) image. With a sufficiently small probe it is possible to achieve an atomic-resolution Z-contrast image in which atomic columns are seen bright (consistent with it being a dark-field image) and their relative contrast is approximately given by their projected mean square atomic number. The atomic-resolution contrast again comes from the interference of diffracted beams, except that no phase plates are necessary to create the intensity. The total intensity on the detector rises and falls as the probe scans the lattice because of interference between the diffracted beams reaching the detector, as shown in **Figure 3a**. Each beam takes the form of a disk the size of the objective aperture (the incident beam in STEM). Interference occurs wherever the disks overlap and there are two or more different pathways that can interfere. The conditions for optimum defocus are that the entire area of overlap shows the strongest possible interference as the probe scans. This is quite different from the conditions for optimum phase contrast with a (small) bright-field detector, and for the example depicted, the bright-field detector covers no overlaps and will show no image.

Smaller spacings will give diffraction disks further apart with smaller regions of overlap and lower

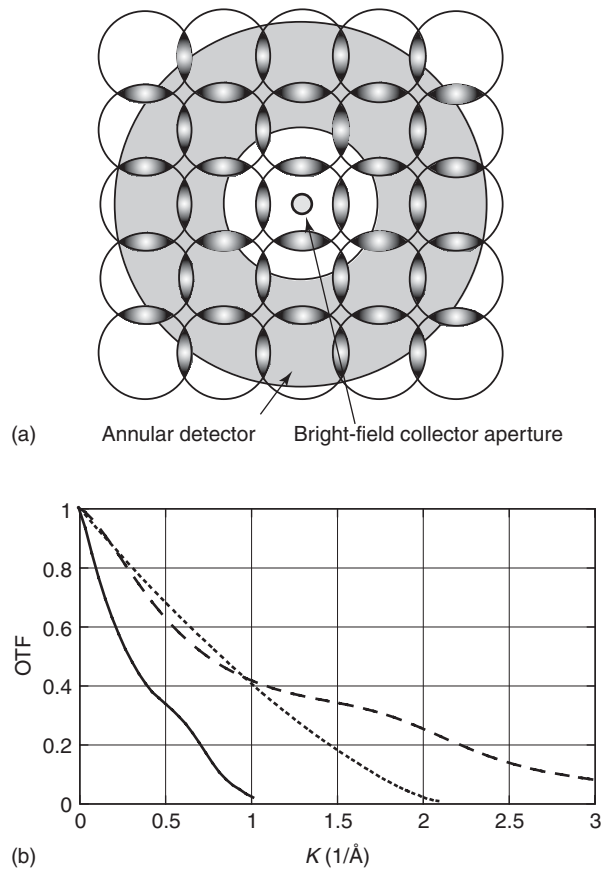

Figure 3 (a) Schematic showing overlapping diffraction disks on the STEM annular detector. The regions of overlap show interference as the probe scans leading to an atomic resolution image. Note, for the spacings depicted, the bright-field detector covers no overlaps and shows no image. (b) Incoherent object transfer functions for an uncorrected 300 kV STEM: solid line (conditions correspond to those in **Figure 2** except $\Delta f = -34$ nm), a corrected 300 kV STEM; dotted line (as **Figure 2** except $\Delta f = 2$ nm), a 200 kV STEM with correction up to 5th order; dashed line (as **Figure 2** except $\Delta f = 0$ nm).

maximum contrast. The incoherent transfer function is therefore a slowly decreasing function of spatial frequency, and is obtained from the Fourier transform of the image intensity,

$$I(\boldsymbol{K}) = O(\boldsymbol{K}) \cdot |P(\boldsymbol{K})|^2$$

The transfer function is just the Fourier transform of the probe intensity, and is referred to as a modulation transfer function, $|P(\boldsymbol{K})|^2$, or object transfer function. Generally, this remains a positive function even as defocus is varied so inverted contrast is not observed. **Figure 3b** shows incoherent transfer functions corresponding to the coherent contrast transfer functions of **Figure 2c**.

Figure 4 compares aberration-corrected coherent and incoherent images of $SrTiO_3$ in the $\langle 1\,1\,0 \rangle$

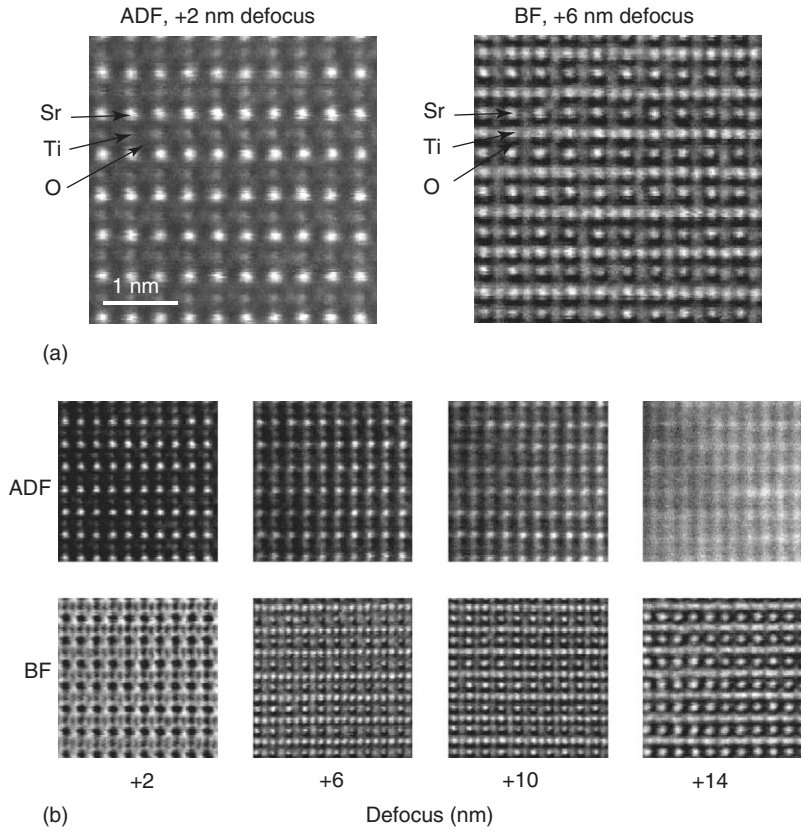

Figure 4 Comparison of incoherent and coherent imaging of $SrTiO_3$ in the ⟨1 1 0⟩ projection in a 300 kV aberration-corrected STEM (a VG Microscope's HB603U with Nion aberration corrector, conditions as in **Figures 2** and **3**). A defocus series was taken using ADF and coherent BF detectors simultaneously. (a) The ADF image shows good *Z*-contrast, with O barely visible. The phase contrast BF image shows the O columns with high contrast; however, the bright features between the Sr columns are double periodicity artifacts. (b) A through focal series with 4 nm defocus steps from the position of optimum ADF defocus showing how the incoherent ADF image contrast slowly blurs while the phase contrast image shows many different forms of contrast. Images are raw data and show some instabilities. (Courtesy of M F Chisholm, A R Lupini, and A Borisevich.)

projection, obtained simultaneously in an aberration-corrected STEM. There is one optimum focus for the *Z*-contrast image, where the Sr column is brightest and the TiO column less bright. A small peak is present at the oxygen column position but is difficult to detect above the noise because of its low *Z*. In the phase contrast image, a good image of the oxygen columns is obtained at a defocus of +6 nm, but other images are seen at other defocus values.

The TEM as a Nano-Laboratory

The TEM is a very versatile instrument and is more like a nano-laboratory than an optical instrument, with a large array of imaging and spectroscopic methods available to probe materials at the atomic scale. Imaging modes are available for magnetic fields (Lorentz imaging, Foucault imaging, holography), and movies have been taken of flux line motion in superconductors. Many applications desire measurements under conditions other than the high vacuum, room temperature environment that is standard for TEM; phase transformations can be observed with a heating holder; studies of catalysis benefit from imaging in an active gas environment; many condensed matter physics investigations require low temperatures; nanowires can be observed while being stretched with simultaneous measurement of conductance. *In situ* microscopy also benefits from aberration-correction because it is possible to maintain resolution with a larger gap between the objective lens pole pieces.

Future Directions

The achievement of aberration-correction in TEM is likely to be seen as one of the most significant events in the history of the microscope. Aberration-correction substantially improves vision at the atomic scale, through better resolution and better contrast, for the first time giving useful sensitivity to single atoms within materials and on their surfaces.

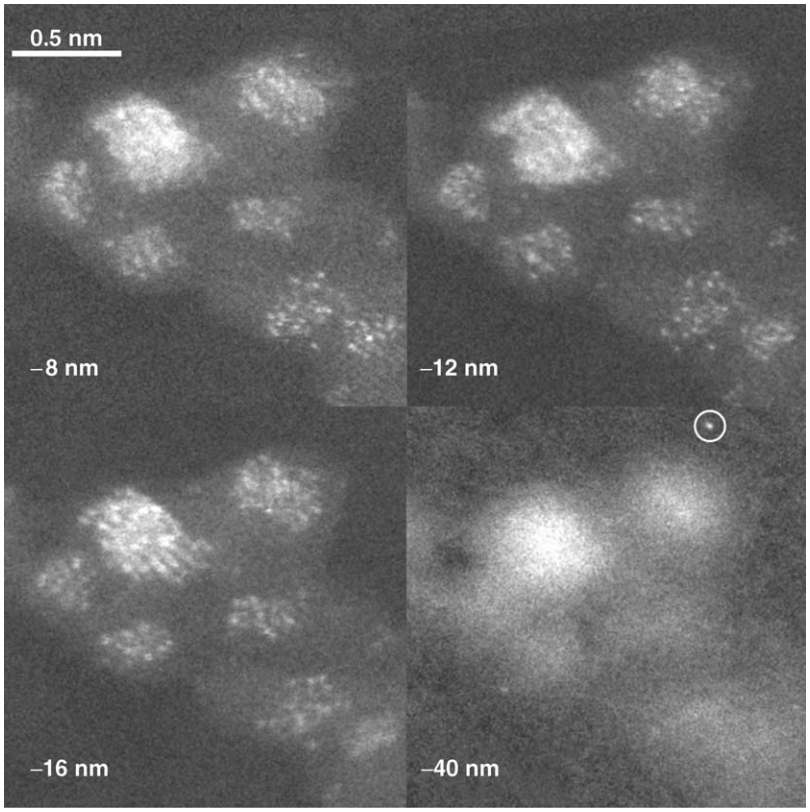

Figure 5 Four frames from a through-depth series of ADF images of a Pt_2Ru_4 catalyst supported on γ-alumina taken using a 300 kV VG Microscope's HB603U with Nion aberration corrector. The alumina is three-dimensional with thin, raft-like Pt–Ru clusters on its surface. Pt atoms are brighter spots and Ru atoms are less bright. Different clusters are resolved at different depths, until, at -40 nm defocus, the carbon support film is reached and a single Pt atom comes into focus (circled). (Image courtesy A Borisevich and A R Lupini.)

Equal improvements apply to spectroscopy. These developments promise a new level of insight into the physics of interfaces, defects, and nanostructures, issues relevant to the majority of materials and devices of a technological world.

A TEM image presents a 2D projection of a 3D specimen. Stereo techniques have been used to obtain information on the third dimension, and recently, full 3D tomography has been demonstrated at nanometer resolution from a series of images taken over a large range of sample tilts. Aberration-correction allows larger objective aperture angles to be utilized, and sub-nanometer depth resolution with sub-Ångstrom lateral resolution is likely to be achieved within the next few years. This allows the possibility of 3D STEM through depth slicing. Just as in optical confocal microscopy, a series of images taken at different focus settings can be reconstructed into a 3D object. **Figure 5** shows four sections of a 3D data set showing catalyst atoms at different depths on a high surface area alumina support.

See also: Confocal Optical Microscopy; Low-Energy Electron Microscopy; Optical Microscopy; Photoelectron Spectromicroscopy; Scanning Near-Field Optical Microscopy; Scanning Probe Microscopy; Scattering, Elastic (General).

PACS: 68.37.Lp; 61.14.−x; 61.46.+w; 61.72.−y

Further Reading

Egerton RF (1996) *Electron Energy-Loss Spectroscopy in the Electron Microscope*, 2nd edn. New York: Plenum.

Kirkland EJ (1998) *Advanced Computing in Electron Microscopy*. New York: Plenum.

Peng L-M, Dudarev SL, and Whelan MJ (2004) *High-Energy Electron Diffraction and Microscopy*. Oxford: Oxford University Press.

Reimer L (2005) *Transmission Electron Microscopy*. Berlin: Springer.

Rickerby DG, Valdré U, and Valdré G (1999) *Z-Contrast Scanning Transmission Electron Microscopy*. Dordrecht: Kluwer.

Spence JCH (2003) *High Resolution Electron Microscopy*. Oxford: Oxford.

Wang ZL (1995) *Elastic and Inelastic Scattering in Electron Diffraction and Imaging*. New York: Plenum.

Williams DB and Carter CB (1996) *Transmission Electron Microscopy*. New York: Plenum.

Zhang X-F and Zhang Z (2001) *Progress in Transmission Electron Microscopy*. Berlin: Springer.